

The phase diagram of molten randomly grafted copolymers

Shuyan Qi and Arup K. Chakraborty

Department of Chemical Engineering, Department of Chemistry, and Materials Science Division, Lawrence Berkeley National Laboratory, University of California, Berkeley, California 94720

(Received 4 December 2000; accepted 8 May 2001)

We study the microphase segregation of molten randomly grafted copolymers (RGCs) using a Landau field theory. Under one wave number approximation, we find three equilibrium ordered microphases: lamellar phase (LAM), hexagonal cylinder phase (HEX), and bcc sphere phase (BCC). The stability of these phases strongly depends on the architectural parameters describing the RGC chains (e.g., the backbone length, the branch length, and the number of branches). Our calculation reveals that RGCs with high average composition of backbone monomers or with low branching density tend to form LAM microstructures. For a small average composition of backbone monomers, HEX and BCC microphases appear in turn with increasing branching density. Independent of the architectural parameters and composition, the disorder to order transition for molten RGCs is always from the disordered phase to the LAM microphase. The physical reasons underlying this behavior and experimentally testable predictions are discussed. © 2001 American Institute of Physics. [DOI: 10.1063/1.1382857]

I. INTRODUCTION

In recent years, much interest has been directed toward understanding how copolymers with incompatible segments can self-organize to form ordered microstructures. Such microstructured materials can prove useful in applications,¹ and so there is a practical motivation for studying this class of phenomena. Many fundamental issues need to be clarified in order to understand the self-organization characteristics of copolymers. Past research efforts have elucidated how structural features and the chemistry of copolymers can be manipulated to tune the nature of the self-assembled microstructures that result upon cooling below a certain temperature. For example, in diblock copolymers, the average composition can be tuned to vary the size of the microstructured domains as well as the symmetry of the ordered microphases.^{2,3} Another “knob” that can be used to dial in desired microstructures, and hence properties, is the sequence of copolymers. For example, work on triblock copolymers with three kinds of segments suggests that a vast array of microphases can result in these systems.⁴ Theoretical work has also predicted that varying the sequence statistics of linear random copolymers (LRCs) results in changes in the microphase separation temperature (MST) and the sizes of the microdomains.^{5–16} Unfortunately, these interesting predictions for the microphase ordering characteristics of LRCs have not been tested experimentally because of difficulties associated with carefully controlling the sequence statistics of synthetic LRCs.

Recently, we studied a class of random copolymers that can be synthesized with careful control of sequence statistics.^{17,18} These are polymers with a homopolymeric backbone with chains of another homopolymer grafted on to the backbone. The branch points are distributed in a random sequence. These randomly grafted copolymers (RGCs) are synthesized by a combination of anionic polymerization and

selective silane coupling.¹⁹ For RGCs with an uncorrelated (i.e., random) distribution of branch points, there are three parameters that can be manipulated to affect the microphase ordering characteristics: the length of the backbone (N), the length of the branches (M), and the number of branches (P). In recent publications,^{17,18} we have demonstrated that the domain size of RGCs, in the vicinity of the MST, is a strong function of temperature, and that N , M , and P strongly influence the microphase ordering characteristics. These studies suggest that RGCs constitute a copolymeric system with a number of architectural parameters that can be manipulated synthetically to change the properties of microphase ordered phases. Furthermore, changing the statistics of the sequence of branch point locations could augment the degree of control on the microphases.

This paper is organized as follows. In Sec. II, we briefly describe our model for molten RGCs and the free energy functional derived in detail in Ref. 18. In Sec. III, this free energy functional is employed to investigate the equilibrium microphases in the one wave number approximation and weak segregation limit. We only consider the lamellar (LAM), hexagonal cylinder (HEX), and spherical bcc (BCC) microphases. The physical reasons which underlie the novel aspects of the predicted phase diagram (e.g., re-entrant phases) are also discussed in Sec. III. Brief concluding remarks are offered in Sec. IV. Here we also point out that formation of microphases with the symmetries that we study could be pre-empted by macroscopic phase separation. Such macroscopic phase separation has been predicted for LRCs. We do not study macroscopic phase separation in this paper, although our free energy functional could be employed for such an investigation. While we hope to carry out such studies in the future, this paper provides us with the specific symmetry of the microphase that would compete with macrophase separation under different conditions.

II. MODEL

The system we consider consists of N_c RGC chains. The positions of the branch points for a specific chain are quenched. We emphasize that each chain has a different sequence of branch points, but all sequences belong to the same statistical distribution. Specifically, we consider a distribution where the average distance between adjacent branch points is N/P , and the fluctuations in branch point locations exhibit short-range correlations.

$$\begin{aligned} \left\langle \frac{F}{V} \right\rangle = & \frac{1}{2} \int d\mathbf{q} \left[\frac{\sum_{i,j=1}^2 M_{ij}(\mathbf{q})}{\det M(\mathbf{q})} - 2\chi/(N+PM) \right] m(\mathbf{q})m(-\mathbf{q}) - \frac{1}{6} \int d\mathbf{q}_1 d\mathbf{q}_2 \Gamma_3(\mathbf{q}_1, \mathbf{q}_2) m(\mathbf{q}_1) m(\mathbf{q}_2) m(-\mathbf{q}_1 - \mathbf{q}_2) \\ & - \frac{1}{24} \int d\mathbf{q}_1 d\mathbf{q}_2 d\mathbf{q}_3 \Gamma_4(\mathbf{q}_1, \mathbf{q}_2, \mathbf{q}_3) m(\mathbf{q}_1) m(\mathbf{q}_2) m(\mathbf{q}_3) m(-\mathbf{q}_1 - \mathbf{q}_2 - \mathbf{q}_3) \\ & + \frac{1}{8} \left\{ \left\langle \left[\int d\mathbf{q} \frac{\sum_{i,j=1}^2 M_{0ij}(\mathbf{q})}{\det M_0(\mathbf{q})} m(\mathbf{q})m(-\mathbf{q}) \right]^2 \right\rangle - \left\langle \int d\mathbf{q} \frac{\sum_{i,j=1}^2 M_{0ij}(\mathbf{q})}{\det M_0(\mathbf{q})} m(\mathbf{q})m(-\mathbf{q}) \right\rangle^2 \right\}, \end{aligned} \quad (1)$$

where $m(\mathbf{q})$ is the order parameter defined by $m(\mathbf{r}) = \xi_B \rho_A(\mathbf{r}) - \xi_A \rho_B(\mathbf{r})$, with ξ_A and ξ_B being the average compositions of monomer A and B , and $\rho_A(\mathbf{r}) = \sum_{i=1}^N \int dn \delta[\mathbf{r} - \mathbf{r}_i(n)]$ and $\rho_B(\mathbf{r}) = \sum_{i=1}^N \sum_{j=1}^P \int ds \delta[\mathbf{r} - \mathbf{r}_{ij}(s)]$ are the coarse-grained macroscopic densities of monomer A and B . χ is the Flory–Huggins parameter. The cubic ($\Gamma_3(\mathbf{q}_1, \mathbf{q}_2)$) and quartic ($\Gamma_4(\mathbf{q}_1, \mathbf{q}_2, \mathbf{q}_3)$) coefficients and the 2×2 matrices M and M_0 are described in detail in the previous paper.¹⁸ The quartic term is written as a sum of two terms. The first term (the term contains $\Gamma_4(\mathbf{q}_1, \mathbf{q}_2, \mathbf{q}_3)$) is related to the average of the random distribution of branch points. The second term is directly related to the quenched fluctuations of this random distribution. For regularly grafted copolymers, the second term is equal to zero.

The quadratic coefficient in Eq. (1) is related to the structure factor in the *disordered* state. To study microphase ordering of RGC melts, cubic, and quartic terms are crucial. By comparing the free energy obtained from Eq. (1) for microphases with different symmetries, we are able to obtain the equilibrium microphases for RGCs with different architectural parameters and construct the phase diagram.

To illustrate the essential phase behavior of molten RGCs, we shall restrict ourselves to the one wave number approximation. This means we shall only consider microstructures with $|\mathbf{q}| = q^*$ (q^* is the optimal wave vector that minimizes the free energy). This approximation is justified in the weak segregation limit (WSL) where the amplitude for compositional variation is small and there are no sharp interfaces between A -rich and B -rich domains. Therefore, the phase behavior is mainly determined by the first set of harmonic waves in the reciprocal lattice. Basically, we define:

$$m(\mathbf{q}) = \sum_{\{\mathbf{G}\}} A \delta(\mathbf{q} - \mathbf{G}), \quad (2)$$

where $\{\mathbf{G}\}$, with $|\mathbf{G}| = q^*$, is the first set of wave vectors in the reciprocal lattice for a specific microstructure. Based on

For the system described above, we have derived the free energy functional previously.^{17,18} This is achieved by using a cumulant method in a field theoretical framework^{2,20} and by employing the replica trick to carry out the quenched average over the random distribution of branch points.²¹ We also set the volume of the system $V = N_c(N + PM)$ (lattice model) such that the monomer density $\rho_0 = N_c(N + PM)/V = 1$. The free energy functional for an incompressible melt, $\rho_A(\mathbf{r}) + \rho_B(\mathbf{r}) = \rho_0 = 1$, is found to be:

this, we can obtain the equilibrium wave amplitude A and the optimal wave vector q^* by minimizing the free energy functional in Eq. (1) with respect to the two parameters.

With the one wave number approximation, Leibler² has shown that three equilibrium microstructures are most likely to form upon traversing the MST: LAM, HEX, and BCC. We employ Eqs. (1) and (2) to identify the microphase with the lowest free energy among these three microstructures and the disordered phase (DIS) for RGCs with different chain architectural parameters.

III. RESULTS AND DISCUSSIONS

By considering the scaling transformation $N' = \xi N$, $M' = \xi M$ and $P' = P$, we can prove that, two out of the three parameters, N , M , and P , are sufficient to describe the microphase ordering of RGCs.¹⁸ We shall choose P/N (branching density) and $f_A = N/(N + PM)$ (average composition of backbone monomers) to characterize the chain architecture. Figures 1–5 contain our main results regarding the phase diagrams of molten RGCs. Each of these figures depicts the χ - P/N phase plane for different compositions, f_A . We fix the backbone length N and the product PM while changing P/N . Thus different values of P/N in the phase plane also correspond to different values of M . Changes in f_A (Figs. 1–5) correspond to different values of PM .

In Fig. 1(a), we show the phase diagram with $f_A = N/(N + PM) = 0.19$. Three ordered equilibrium phases are predicted. For small values of P ($P < 10$) and at low temperature, the LAM morphology is preferred. Also, the LAM and HEX microphases are separated by a steep phase boundary with respect to the change in P/N . For large values of P ($P > 20$), the HEX microstructure is preferred at low temperature while the BCC microstructure is preferred within a higher temperature window. For intermediate values of P ($10 < P < 20$), the HEX microphase is the equilibrium mi-

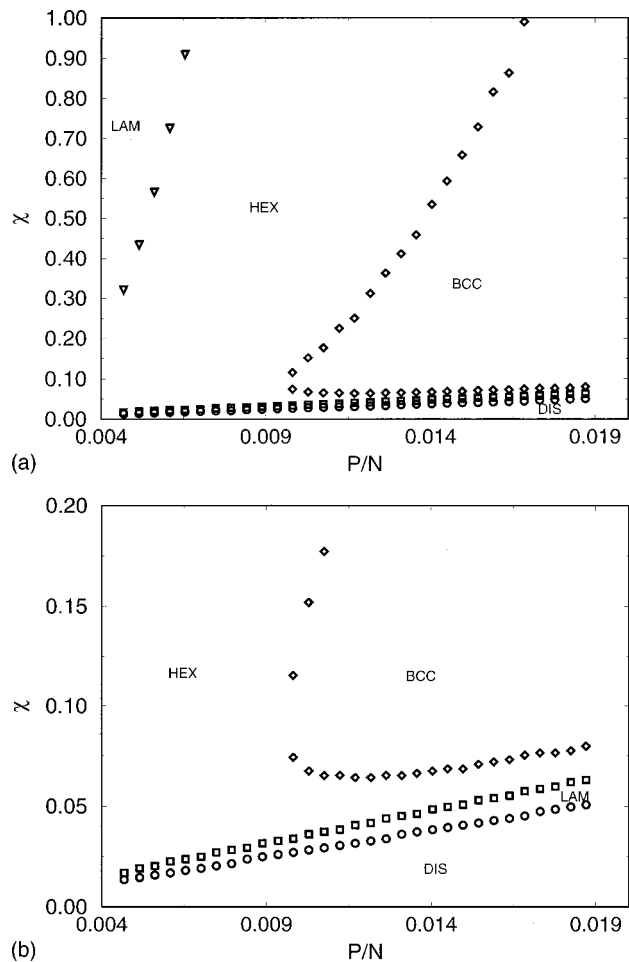


FIG. 1. (a) The phase diagram for RGCs with $f_A=0.19$. The values of P/N are chosen such that $N=2138$ and P ranges from 10 to 40. The details of the phase diagram close to the MST are shown in (b).

crostructure within a large temperature window. Figure 1(b) shows a more detailed picture of the phase plane close to the MST value. For $P < 20$, as temperature increases, the HEX microstructure becomes unfavorable to LAM. The order-disorder phase transition is thus always between LAM and

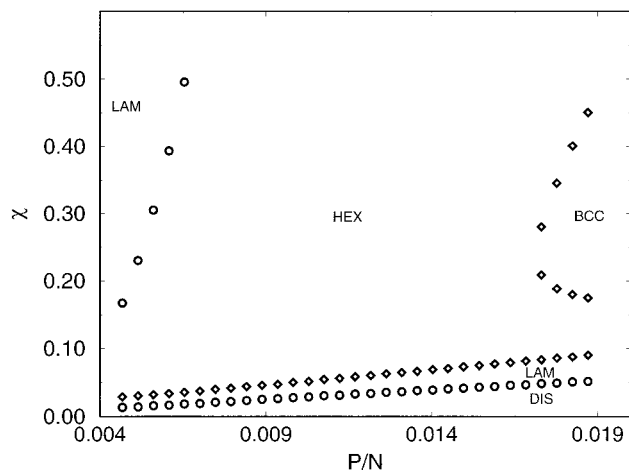


FIG. 2. The phase diagram for RGCs with $f_A=0.25$. The values of P/N are chosen such that $N=2138$ and P ranges from 10 to 40.

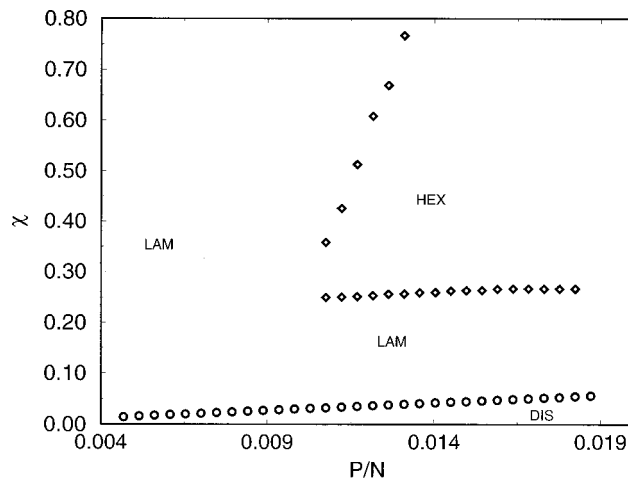


FIG. 3. The phase diagram for RGCs with $f_A=0.32$. The values of P/N are chosen such that $N=2138$ and P ranges from 10 to 40.

DIS. For $P > 20$, close to the order-disorder phase boundary and in the direction of increasing temperature, BCC, HEX, and LAM microstructures are encountered, in turn, as equilibrium microphases. The order-disorder phase transition is again from LAM to DIS. (We will return to the issue of the re-entrance to a LAM microstructure later.) In this narrow temperature window close to MST, our theory indicates that the free energy of the three ordered phases are very close ($\Delta F/F < 0.0001$). Since it is experimentally difficult to distinguish different phases according to such tiny differences in the free energy, our prediction of the phase diagram very close to the MST is tentative.

In Fig. 2, we show the phase diagram for $f_A=0.25$. The results are similar to those depicted in Fig. 1. LAM is the equilibrium microphase at small values of P/N and at low temperature, and BCC is preferred within a temperature window at high values of P/N . The HEX microphase is the equilibrium microstructure for intermediate values of P/N within a large temperature window. However, we find the phase boundaries for LAM-HEX and HEX-BCC at low temperature are shifted to higher values of P/N compared to

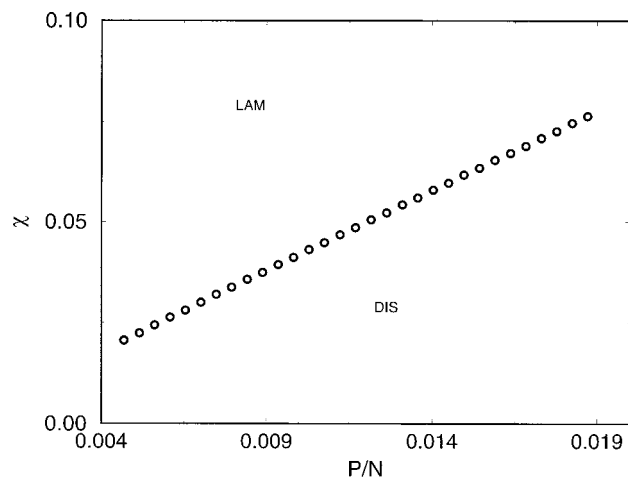


FIG. 4. The phase diagram for RGCs with $f_A=0.49$. The values of P/N are chosen such that $N=2138$ and P ranges from 10 to 40.

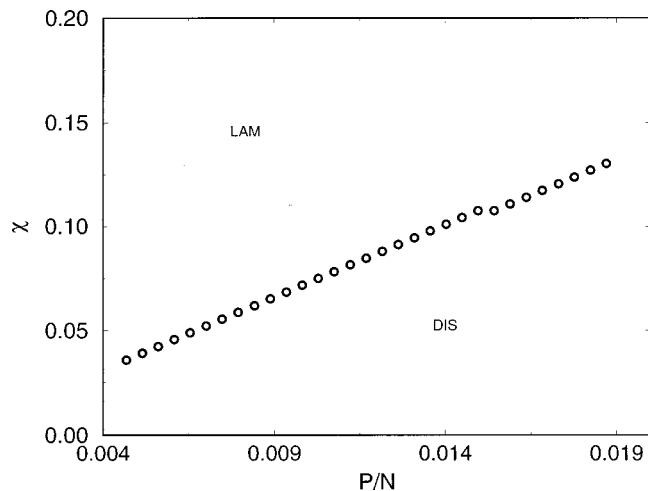


FIG. 5. The phase diagram for RGCs with $f_A=0.66$. The values of P/N are chosen such that $N=2138$ and P ranges from 10 to 40.

Fig. 1. The region where LAM is the equilibrium microphase close to the MST is also much larger. This trend continues as we increase f_A to 0.32, shown in Fig. 3. The shift of the low temperature LAM-HEX phase boundary to higher values of P/N and the expansion of the region between HEX and DIS where LAM is preferred (close to MST) are more obvious; the two regions where LAM is the equilibrium microphase merge into one in the phase diagram (for $10 < P < 40$). Also, the shift of the HEX-BCC phase boundary removes the BCC microphase as an equilibrium microstructure within the range of P shown in the phase diagram ($10 < P < 40$). Finally, in the case of $f_A=0.49$ and $f_A=0.66$ (shown in Figs. 4 and 5), we only find the LAM microstructure as an equilibrium microphase within this range of P ($10 < P < 40$).

The physical reasons underlying why LAM, HEX, and BCC microstructures in turn become the equilibrium microphase when P/N increases (see Figs. 1 and 2) are as follows. For a fixed value of f_A , increasing P while keeping PM a constant corresponds to an architecture change which makes the RGCs more brushlike (see Fig. 6). To understand how this architectural change affects RGC phase behavior, we consider the conformational entropy attributed to a spe-

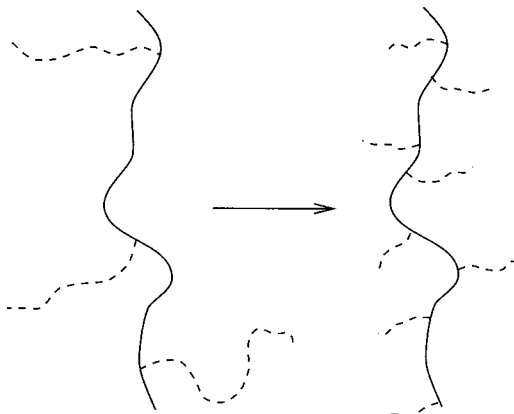


FIG. 6. A sketch showing an increase in the branching density P/N of randomly grafted copolymers (RGCs) with keeping $f_A=N/(N+PM)$ constant.

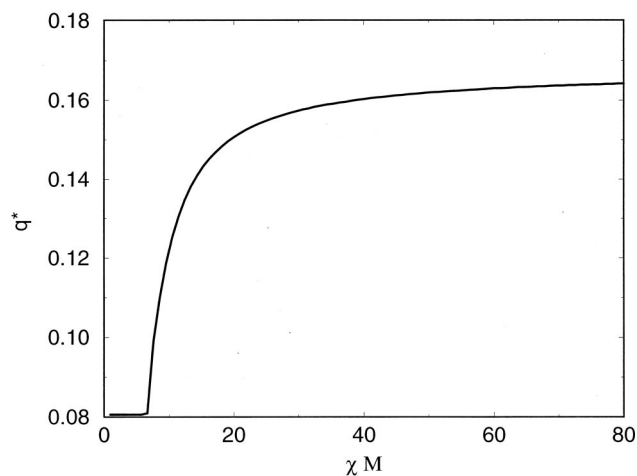


FIG. 7. The temperature dependence of the optimal wave vector q^* for RGCs with $N=2138$, $M=285$, and $P=16$.

cific microstructure. For brushlike RGCs, there are more branch points on a chain. It is entropically more favorable to form a spherical interface rather than a planar interface because this allows the backbone monomers to be inside the spherical domains (for $f_A < 0.5$), and thus avoids the dominant entropic penalty associated with forming loops necessary when the backbone monomers form the matrix. In other words, brushlike RGCs prefer an isotropic and more symmetrical interface in order to minimize conformational entropy cost. Therefore, BCC and HEX microphases are favored over LAM when P/N is large. Also, because the branch monomers are forced to mix with backbone monomers to a larger degree for brushlike RGCs, it is harder for the system to segregate. Thus the MST curve tilts in the direction of lower temperatures for RGCs with larger values of P/N .

When very close to the MST, another entropic effect becomes important and causes reentrance to the LAM microphase [see Fig. 1(b) and Fig. 2]. Recall that, near the MST, our theory^{17,18} predicts that the optimal wave vector q^* decreases when temperature increases (Fig. 7). At low temperature, q^* is equal to an asymptotic value q_f . Increasing temperature results in a decrease in q^* , but the change in q^* is sharp only in a narrow window immediately below the MST.^{17,18} At the MST, $q^*=q_c$, where q_c is the optimal wavevector for composition fluctuations in DIS. Therefore, immediately below the MST, by increasing temperature, the entropy associated with stretching polymer chains suddenly becomes significant. For a fixed change in q^* , the chain deformation because of the increasing domain size for LAM, HEX, and BCC microstructures is in the ratio $1:2/\sqrt{3}:\sqrt{3}/\sqrt{2}$ (by comparing the spacing between adjacent domain centers). Thus the LAM microphase has the advantage of contributing the smallest entropy cost due to this deformation. This is why we find that the LAM microphase reappears close to the MST before the transition to DIS. Since the window in which q^* changes is wider for more brushlike RGCs,¹⁸ we see a broader range of phase space wherein the LAM microphase is the equilibrium phase when P/N is large.

We want to call attention to the fact that the order–disorder phase transition, as predicted by this Landau field theory, is always between LAM and DIS. This means that the order–disorder phase transition for RGCs is always of second order. The order–disorder microphase transition for LRC melts is also not first order; only when macrophase separation occurs is the transition first order.^{13–16} This is in contrast with mean field predictions for molten DCPs² where, for compositionally asymmetric DCPs, the order–disorder phase transition is between DIS and BCC. This is a first order transition. The origin of higher order phase transitions in RGCs and LRCs seems to be related to the quenched randomness which gives rise to continuous choices of the domain spacing. This allows chains with disordered sequence to decrease the energetic driving force in a smooth manner as opposed to chains with ordered sequence wherein a natural length scale is prescribed.

Figures 1–5 show that the LAM region in the phase diagram expands by increasing the average composition of backbone monomers, f_A . To understand this, we first consider the situation when the branch monomers constitute the majority component ($f_A < 0.5$). In this case, for circular (or spherical) morphologies such as HEX (or BCC), branch monomers form the matrix while backbone monomers are inside the circular (or spherical) microstructure. When f_A approaches 0.5, because the volume fractions of monomer A and monomer B are comparable, the LAM microstructure is favored over curved morphologies. This is also demonstrated by DCPs² and ABA triblock copolymers.²² However, we find that for RGCs the LAM microphase also dominates the phase diagram when $f_A > 0.5$. The reason behind this is that backbones and branches are topologically different. When $f_A > 0.5$, to form a circular (or spherical) microstructure such as HEX (or BCC), the branch monomers are inside the circular (or spherical) structure while the backbone monomers form the matrix. The backbone monomers have to form loops with their ends located at the interfaces. This entropic cost associated with making loops when the backbone monomers comprise the matrix is large and causes the system to form morphologies with planar interfaces. Thus when $f_A > 0.5$, the phase diagram is dominated by regions corresponding to the LAM microphase.

IV. CONCLUSIONS

In this paper, we use the Landau free energy functional for molten RGCs derived earlier^{17,18} to investigate the phase diagram. Under the one wave number approximation, we construct the phase diagram for different architectures of RGCs. We find three possible ordered equilibrium microphases: LAM, HEX, and BCC. We focus our discussion on the effects of changing branching density (P/N) and average composition of backbone monomers (f_A). We find a strong dependence of the phase behavior on these parameters. For example, for small values of f_A , chemically identical systems will form LAM, HEX, and BCC microphases

in turn as the branching ratio is increased. In contrast, for large values of f_A , the only ordered equilibrium microphase is the LAM microstructure. An intriguing and potentially significant finding is that for RGCs, regardless of the composition, the order–disorder transition is always between DIS and LAM. As a consequence, re-entrant behavior passing from HEX to LAM to DIS may result as temperature is increased. This also implies that, within mean field theory, order–disorder transitions for RGCs are always continuous. This (in contrast with the well-studied phase behavior of block copolymers with ordered sequences) is the result of the quenched random sequence of branch points in RGC chains. We hope this study will stimulate experimental investigations of the equilibrium phase diagram of RGC melts.

ACKNOWLEDGMENTS

Financial support is provided by U.S. D.O.E. (Basic Energy Sciences). The authors are very grateful to Professor N. P. Balsara and Professor E. I. Shakhnovich for numerous fruitful discussions and collaborations on the physics of RGCs.

- ¹M. Park *et al.*, *Science* **276**, 1401 (1997); R. Langer, *Nature (London)* **392**, 6679 (1998); A. S. Tse, Z. J. Wu, and S. A. Asher, *Macromolecules* **28**, 6533 (1995).
- ²L. Leibler, *Macromolecules* **13**, 1602 (1980).
- ³F. S. Bates and G. H. Fredrickson, *Annu. Rev. Phys. Chem.* **41**, 525 (1990); G. H. Fredrickson and F. S. Bates, *Annu. Rev. Mater. Sci.* **26**, 501 (1996).
- ⁴W. Zheng and Z.-G. Wang, *Macromolecules* **28**, 7215 (1995).
- ⁵A. Sali, E. I. Shakhnovich, and M. Karplus, *Nature (London)* **369**, 248 (1994).
- ⁶H. Frauenfelder and P. G. Wolynes, *Phys. Today* **47**, 57 (1994).
- ⁷H. S. Chan and K. A. Dill, *Phys. Today* **46**, 24 (1993).
- ⁸D. Bratko, A. K. Chakraborty, and E. I. Shakhnovich, *Phys. Rev. Lett.* **76**, 1844 (1996).
- ⁹S. Srebnik, A. K. Chakraborty, and E. I. Shakhnovich, *Phys. Rev. Lett.* **77**, 3157 (1996).
- ¹⁰E. I. Shakhnovich and A. M. Gutin, *J. Phys. (Paris)* **50**, 1843 (1989).
- ¹¹G. H. Fredrickson and S. T. Milner, *Phys. Rev. Lett.* **67**, 835 (1991); G. H. Fredrickson, S. T. Milner, and L. Leibler, *Macromolecules* **25**, 6341 (1992).
- ¹²A. M. Gutin, A. Yu. Grosberg, and E. I. Shakhnovich, *Macromolecules* **26**, 3598 (1993).
- ¹³S. V. Panyukov and I. I. Potemkin, *JETP Lett.* **64**, 197 (1996); S. V. Panyukov and I. I. Potemkin, *JETP* **85**, 183 (1997); *ibid.* **85**, 183 (1997); I. I. Potemkin and S. V. Panyukov, *Phys. Rev. E* **57**, 6902 (1998); S. V. Panyukov and I. I. Potemkin, *Phys. A* **249**, 321 (1998).
- ¹⁴A. Nesarikar, M. O. dela Cruz, and B. Crist, *J. Chem. Phys.* **98**, 7385 (1993).
- ¹⁵A. V. Dobrynin and L. Leibler, *Europhys. Lett.* **36**, 283 (1996); A. V. Dobrynin, *J. Chem. Phys.* **107**, 9234 (1997).
- ¹⁶H. J. Angerman, G. tenBrinke, and I. Erukhimovich, *Macromolecules* **29**, 3255 (1996); *ibid.* **31**, 1958 (1998); H. J. Angerman, G. tenBrinke, and J. M. Slot, *Euro. Phys. Journ. B* **12**, 397 (1999).
- ¹⁷S. Qi, A. K. Chakraborty, H. Wang, A. A. Lefebvre, N. P. Balsara, E. I. Shakhnovich, M. Xenidou, and N. Hadjichristidis, *Phys. Rev. Lett.* **82**, 2896 (1999).
- ¹⁸S. Qi, A. K. Chakraborty, and N. P. Balsara, *J. Chem. Phys.* **115**, 3387 (2001), preceding paper.
- ¹⁹M. Xenidou and N. Hadjichristidis, *Macromolecules* **31**, 5690 (1998).
- ²⁰K. M. Hong and J. Noolandi, *Macromolecules* **14**, 727 (1981).
- ²¹S. F. Edwards and P. W. Anderson, *J. Phys. (Paris)* **5**, 965 (1975).
- ²²M. W. Matsen and R. B. Thompson, *J. Chem. Phys.* **111**, 7139 (1999).